SINGLE-BUNCH INSTABILITY OF POSITRON BEAMS IN ELECTRON CLOUD

K. V. Lotov*, BINP, 630090, Novosibirsk, Russia
G. V. Stupakov, SLAC, Stanford, CA 94305, USA

Abstract

Single-bunch instability of a short and dense positron beam in a photo-electron plasma is studied numerically using code LCODE. The code was originally developed for studies of plasma wakefield acceleration. It is two-dimensional and fully relativistic, with both the beam and electrons modelled by macro-particles. The instability is shown to affect the rear part of the beam, right after the arrival of nearby electrons to the axis. As the result, the emittance of the whole beam grows exponentially. The instability can be stabilized by an external longitudinal magnetic field. The field does not itself stabilize the instability, but prevents the electrons from going to axis once they are thrown to the wall by the previous bunch.

1 INTRODUCTION

In positron rings of B-factories, the electron cloud (electron plasma) produced due to photoemission and secondary emission can cause a single-bunch instability of the beam [1, 2]. Here we analyze the axisymmetric mode of this instability with two-dimensional, fully relativistic, electromagnetic hybrid code LCODE [3], which was originally developed for simulations of plasma wakefield acceleration. Since the motion of electrons near the beam is essentially non-hydrodynamic, the code was modified to enable the particle (Lagrangian) description of the plasma. To clarify the mechanism of the instability, we first study the beam evolution without synchrotron oscillations and then discuss the role of synchrotron motion. Finally, we examine the influence of a longitudinal magnetic field on the instability.

2 THE CODE

We use the cylindric coordinates (r, φ, z) and the co-moving simulation window (Fig. 1). Since the length scale of beam evolution is much longer than the bunch length, we use the so-called quasi-static approximation. Namely, when calculating the plasma response we consider the beam as "rigid" and find the fields as functions of r and $\xi = z - ct$, where c is the speed of light. Then we use these fields to modify the beam, etc.

The beam is modelled by macro-particles; each one is characterized by r- and ξ-coordinates (r_b and ξ_b), r- and z-momenta (p_{br} and p_{bz}), and angular momentum. The force acting on the beam comes from the plasma fields and the
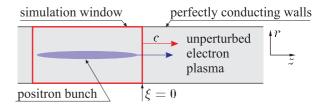
Figure 1: Geometry of the problem.

external focusing:

$$\frac{d\vec{p}_b}{dt} = e(E_r - B_\varphi)\vec{e}_r + eE_z\vec{e}_z - Fr_b\vec{e}_r, \qquad (1)$$

where $\vec{e}_r$ and $\vec{e}_z$ are unit vectors, e is the elementary charge, and F is the external focusing strength.

The fields are obtained from the full Maxwell equations which, in quasi-static approximation, take the form

$$\frac{1}{r}\frac{\partial}{\partial r}rE_r = 4\pi\rho - \frac{\partial E_z}{\partial \xi}, \qquad \frac{1}{r}\frac{\partial}{\partial r}rB_r = -\frac{\partial B_z}{\partial \xi},$$

$$E_\varphi = -B_r, \qquad \frac{\partial(E_r - B_\varphi)}{\partial \xi} = \frac{\partial E_z}{\partial r} = \frac{4\pi}{c}j_r, \quad (2)$$

$$\frac{\partial B_z}{\partial r} = -\frac{4\pi}{c}j_\varphi,$$

where $\vec{j}$ and ρ are the total current and charge densities, respectively.

Plasma macro-particles are characterized by their radius and three components of the momentum. We find these quantities as functions of ξ. Since no information can propagate forward in the simulation window, plasma response and all fields can be found in a single finite-differences passage of the simulation window from right to left.

The boundary conditions for equations (2) are that of a perfectly conducting wall. In front of the bunch the plasma contains uniformly distributed warm electrons and no ions. The electrons incident on the wall are reflected back with the thermal velocity.

3 THE INSTABILITY

Unless stated otherwise, we use the parameters and notation listed in Table 1. It turns out that the wall of the vacuum chamber does not affect the beam evolution, so in simulations we choose a wall of small radius to speed up calculations.

The instability quickly destroys the beam (Fig. 2). We can quantitatively describe this process by tracing the time
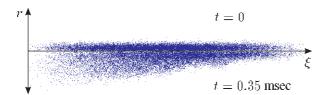
Figure 2: Beam distribution in $r - \xi$ plane for $t = 0$ (top) and $t = 0.35$ msec (bottom) without synchrotron oscillations.
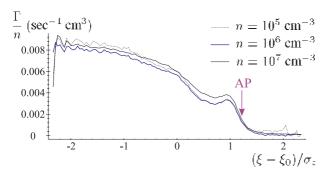

Figure 3: The growth rate of emittance at different beam cross-sections. The beam center is at $\xi = \xi_0$. Arrow shows the arrival point location.
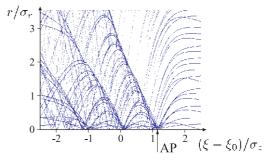

Figure 4: Trajectories of the electrons in calculation window.

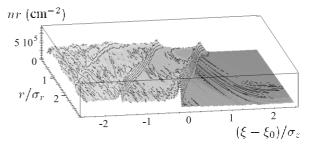Figure 5: The electron density distribution in $r - \xi$ plane. To visualize the off-axis density distribution, the product nr is shown.

dependence of the emittance

$$\epsilon = \frac{c}{W_b} \sqrt{\langle r_b^2 \rangle \left(\langle p_{br}^2 + p_{b\varphi}^2 \rangle \right) - \langle r_b p_{br} \rangle} \tag{3}$$

at various cross-sections of the beam. This dependence turns out to be exponential with the growth rate Γ shown in Fig. 3 by the thick line. The growth rate is directly proportional to the initial electron density, which is seen from comparison of the graphs for several electron densities (thin and dotted lines in Fig. 3).

The observed behavior of the growth rate can be understood from the picture of electron motion (Fig. 4). The electrons are attracted by the bunch electric field. Small imperfections of the field cause small deviations of electron trajectories. Once the electrons arrive to the near-axis region, their electric field affects the positron bunch and heats it due to time-varying field imperfections. The driving force of the instability at a given beam cross-section is thus roughly proportional to the near-beam electron den-

Table 1: Basic set of parameters

Number of particles per bunch, N	10^{11}
Bunch rms radius, σ_r	0.3 mm
Bunch rms length, σ_z	1.3 cm
Bunch-to-bunch distance, L	2.4 m
Beta function (for external focusing)	16 m
Beam energy, W_b	3.1 GeV
Wall radius	0.5 cm
Unperturbed electron density, n_0	10^6 cm^{-3}
Initial electron temperature, T_e	5 eV

sity. If the electron density is lower there (e.g., because of a higher T_e), the growth rate is correspondingly smaller.

Since the beam field is linear in r near the axis, nearby electrons first arrive to the axis almost simultaneously at some point we term "Arrival Point" (AP in Fig. 4). Behind the AP the electron density greatly increases (Fig. 5), and we see the beam breakup there. For a Gaussian beam, the Arrival Point is located exactly at the beam center for

$$\frac{N r_e \sigma_z}{\sigma_r^2} \approx 3.36, \tag{4}$$

where r_e is the classical electron radius. Thus, the instability can manifest itself if the left-hand side of (4) is greater than or of the order of unity.

Note that, as follows from Fig. 5, the electron density near the axis is strongly peaked (as r^{-1}) behind the AP.

From the above consideration it becomes clear why the growth rate is proportional to n_0. Since the self field of electrons is small compared to the beam field, the pattern of electron trajectories and the shape of electron density distribution do not depend on n_0. Hence, the unperturbed electron density affects only the absolute value of the growth rate and not the shape of its ξ-dependence.

To visualize the driving force of the instability, we plot the oscillating part of the focusing force (averaged over the beam radius) as a function of time (over one betatron period) and position along the beam (Fig. 6). The graph is taken at the stage of developed instability. It is seen that ahead of AP there are no force oscillations. Near AP the force oscillates with twice the betatron frequency because of a small mismatch between the beam emittance and the
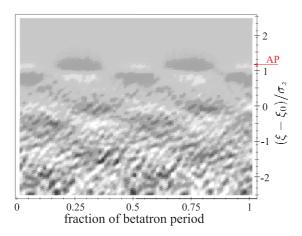
Figure 6: The map of the oscillating part of the focusing force at $t \approx 0.2$ msec.
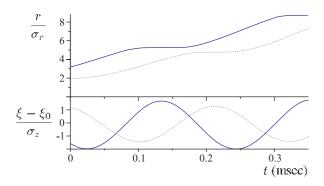

Figure 7: The betatron radius and longitudinal position for two beam particles (a run with synchrotron motion included).

external focusing: electrons "remember" the envelope oscillations of the beam head. Behind the AP the force becomes chaotic and heats the rest of the beam. This is just heating, since no discernible structure is observed on the phase plane (r_b, p_{br}) behind the AP.

The heating model is confirmed by simulations with 20% beam energy spread or 20% energy variation along the beam. In both cases the growth rate was almost the same as for the mono-energetic beam.

The synchrotron motion of the beam, when included, does not affect the growth of the whole beam emittance, but flattens the growth rate profile along the beam if the frequency of synchrotron oscillations is higher than the growth rate. With the synchrotron motion, the radius of particle transverse oscillations increases mostly at the beam tail (Fig. 7). Both observations are in agreement with the heating model.

4 INFLUENCE OF THE LONGITUDINAL MAGNETIC FIELD

Once there are electrons at the beam axis, a longitudinal magnetic field cannot suppress the instability. As follows from simulations, it just reduces the growth rate and some-
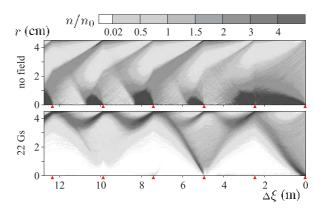

Figure 8: The electron density map for a bunch train in the initially uniform plasma. Triangles show location of the bunches.
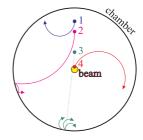

Figure 9: Electron trajectories between successive bunch passages.

what changes the picture of beam breakup. However, the external field can stabilize the beam by preventing electrons from coming to the near-axis area. This effect is observed in modelling of bunch train propagation through an initially uniform electron plasma (Fig. 8). Every bunch delivers a large radial momentum to surrounding electrons. As is illustrated by Fig. 9, in the magnetic field of the strength

$$B_0 = \frac{\pi(2k+1)mc^2}{eL}, \qquad k = 0, 1, 2, \ldots \quad (5)$$

slow electrons (including secondary ones) make half-integer of the cyclotron turn between successive bunches, fast electrons hit the wall, and very few electrons remain on the way of the next bunch. For $L = 2.4$ m we have the minimum optimum field $B_0 = 22$ Gs.

5 ACKNOWLEDGEMENTS

6 REFERENCES

[1] K.Ohmi and F.Zimmermann. Phys. Rev. Lett. **85** (2000), p. 3821.

[2] K.Ohmi et al. Phys. Rev. E **65** (2002), p. 016502.

[3] K.V.Lotov. Phys. Plasmas **5** (1998), p. 785.